Effect of sulfate additions on hydration and performance of ternary slag-limestone composite cements

Samuel Adu-Amankwah[a], Leon Black[a], Jan Skocek[b], Mohsen Ben Haha[b], Maciej Zajac[b]

[a] Institute of Resilient Infrastructure, School of Civil Engineering, University of Leeds, Woodhouse Lane, Leeds, LS2 9JT, UK

[b] Heidelberg Technology Center GmbH, Oberklamweg 2-4, 69181 Leimen, Germany

Abstract

The global cement industry is striving to reduce its carbon footprint. Common approaches have included reduced clinker factors by blending cement clinker with supplementary cementitious materials (SCM). However supplies of SCMs are not sufficient to achieve replacement above about 30 %. Limestone ternary cements offer the opportunity to reduce the clinker factor of cements while maximizing the efficiency of SCMs. In these cements, calcite from limestone reacts with dissolved aluminates to form carboaluminate and in the process influence hydration of other constituents. However, sulfates which are conventionally added to regulate the early reactions in cement also compete for aluminates. Here we have used complementary techniques to investigate the effects of calcium sulfate additions on hydration, microstructure and performance of composite Portland clinker-slag-limestone cements.

The results show that the presence of sulfate influenced the early-age reaction kinetics of the clinker phases and supplementary cementitious materials. However, even after sulfate depletion, the course of hydration and microstructures formed were significantly influenced. Increasing the sulfate level resulted in a gradual increase of the fraction of ettringite over AFm phases, coarser porosity and lower water content of the C-S-H. These microstructural changes impact the total porosity and hence cement strength in opposing ways, namely porosity is reduced with increasing ettringite fraction while the space filling capacity of the C-S-H is also reduced due to the lower water content of the C-S-H. These findings have important implications for optimizing the mechanical properties and durability of ternary blends.

Key words

Ternary blended cements, Limestone, GGBS, PONKCS, Sulfates, Thermodynamic modelling

1. Introduction

Despite many years of research on cement hydration, many phenomena and interactions are still not sufficiently understood. One example is the effect of sulfate on cement hydration and performance. Sulfate is always a component of Portland cement, present as gypsum, basanite (calcium sulfate hemihydrate) or anhydrite. The main role of sulfate is to regulate early-age cement properties [1]. However, the addition of sulfate influences not only the setting time but has also a strong impact on the evolution of the compressive strength of cement mortars and concretes.

Primarily, sulfate reacts with aluminate phases and retards the hydration of C_3A, thus controlling early-age properties [1-3]. The products of the reaction between C_3A (and C_4AF to a lesser extent) and sulfate are initially ettringite and later on monosulfoaluminate. The content of the sulfate thus regulates the balance between the AFt and AFm phases in Portland cement [4]. Hence, the sulfate addition modifies the composition of the phase assemblage, the resulting volume of the hydrates, the remaining porosity

and consequently performance. This is mainly related to the fact that ettringite is characterized by the low density; 1.8 g/cm^3 and has a high bound water content compared to the other AFm phases [5]. Thermodynamic calculations show that an increasing sulfate content leads to the formation of more ettringite and less AFm phases, and thus to a larger hydrate volume and lower porosity [6, 7]. These theoretical observations agree with experimental observations, where in general the formation of more ettringite is accompanied by an increase in compressive strength [6, 8]. However, above 3 – 4 % SO_3 content, a decrease in compressive strength is typically observed [9-11], even though the volume of the hydrates is expected to increase due to greater ettringite formation [1, 6, 8]. The origin of this phenomenon is not yet understood.

The phenomena described are further complicated in the case of composite cements. In this type of cement, additional alumina is provided by cementitious additions such as fly ash [12, 13], slag [7] and calcined clays [14]. This alumina can react with the sulfate. Moreover, modern composite cements contain limestone whose main component is calcite. Ternary limestone blends with aluminosilicate-bearing SCMs and Portland clinker offer the possibility to significantly reduce the clinker fraction of cements [15]. Limestone is a raw material for cement production and it is readily available in most parts of the world. When used without thermal treatment, limestone reduces the clinker factor and hence a lower embodied CO_2 and also maximizes the efficiency of other constituents in composite cements. In this type of composite cements, calcite reacts with the available alumina to form hemi and monocarboaluminate phases instead of the monosulfoaluminate phase [6, 13, 14, 16-18]. This results in ettringite stabilization, decreased porosity and increased strength. In parallel, gradual reaction of the calcite changes the alumina-sulfate balance during the course of hydration. In addition, the presence of limestone may result in an acceleration of the cement clinker and SCM reaction [6, 18]. This means that in systems containing high volumes of supplementary cementitious material, the sulfate content must be carefully adjusted in order to prevent undersulfation and ensure optimal performance [6, 14, 19]. The optimal sulfate levels is generally higher than expected from the cement clinker only [6].

This paper reports on investigations of the interactions of sulfate within ternary slag-limestone composite cements. The impacts of sulfate dosage on hydration kinetics, the hydrated phase assemblages and microstructure are studied. The changes induced by the different sulfate content were correlated with the changes in the compressive strength development. Techniques used include isothermal calorimetry, chemical shrinkage, X-ray diffraction supported by the Rietveld-PONKCS method (QXRD), thermogravimetric analysis (TGA), scanning electron microscopy (SEM-EDS), mercury intrusion porosimetry (MIP) and thermodynamic modelling.

2. Materials and methods

2.1. Materials

Ternary slag-limestone composite cements with a total sulfate content of 2 %, 3 % or 4 % of SO_3 (designated as S-2, S-3 and S-4, respectively) were investigated. In order to prepare the composite cements, industrial CEM I 52.5 R cement, ground granulated blast furnace slag and natural limestone were used. Natural anhydrite additions were used to meet the targeted SO_3 levels.

The chemical composition and specific surface area of the materials, determined by XRF and Blaine measurements respectively, are shown in Table 1. The mineralogical compositions of the cement and the

supplementary materials are shown in Table 2 and Table 3 respectively. The particle size distribution of all the constituent materials, measured by laser granulometry, is shown in Figure 1.

Table 1 Chemical composition (%weight) and Blaine fineness of the investigated materials

Material	CEM I	Slag	Limestone	Anhydrite
SiO_2	20.4	34.9	2.0	2.0
Al_2O_3	5.6	11.6	0.8	0.6
TiO_2	0.3	1.1	0.0	0.0
MnO	0.0	0.3	0.0	0.0
Fe_2O_3	2.5	0.5	0.3	0.2
CaO	62.1	41.8	53.1	38.3
MgO	1.7	5.8	0.6	1.5
K_2O	0.7	0.5	0.1	0.2
Na_2O	0.0	0.0	0.0	0.0
SO_3	3.5	3.1	0.0	52.2
P_2O_5	0.1	0.0	0.0	0.0
LOI	2.0	(+1.45)	42.3	3.7
Blaine Fineness, m^2/kg	593	454	328	472

Table 2 Mineralogical composition of CEM I (%weight)

Phase	C_3S	β-C_2S	C_3A	C_4AF	Calcite	Anhydrite	Hemihydrate	Others
Content (%)	58.1	14.3	9.2	6.7	1.9	1.7	3.0	5.1

Table 3 Mineralogical composition of supplementary materials (%weight)

Phase	Slag (%)	Limestone (%)	Anhydrite (%)
Calcite	2.4	96.6	-
Quartz	0.1	0.4	2.1
Dolomite	-	1	5.5
Anhydrite	-	-	90.7
Gypsum	-	-	1.7
Amorphous	97.5	2	

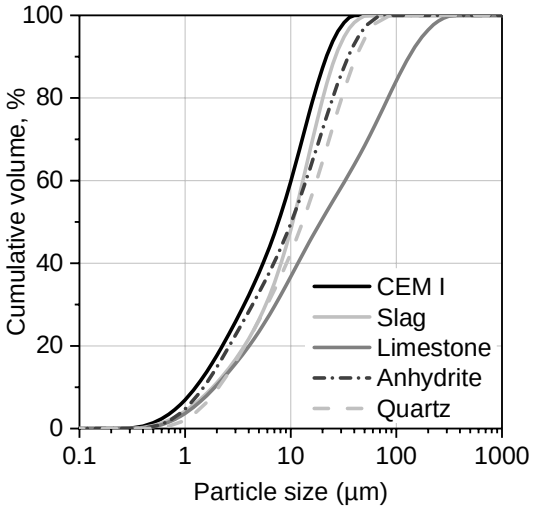

Figure 1 Particle size distribution of constituent materials, determined by laser granulometry.

The mix proportions used are detailed in Table 4. The clinker to SCM ratio was maintained at 50:50, with limestone considered as an SCM where incorporated. The total sulfate contents were attained by adding the required amounts of ground anhydrite. The 1.9 % calcite and the sulfates in the CEM I 52.5 R were accounted for in calculating the total limestone and sulfate contents for the ternary blends. The formulated cements were homogenized in a laboratory ball mill for at least 3 hours, using polymer balls to prevent further grinding of the materials.

Table 4 Composition of mixes investigated (%weight)

Mix designation	Clinker	Slag/Quartz	Calcium carbonate	Sulfate
S-2	49.0	39.2	9.8	2.0
S-3	48.5	38.8	9.7	3.0
S-4	48.0	38.4	9.6	4.0
L	49.1	39.3	9.8	1.8

Note: Calcium carbonate is that in CEM I and added limestone; Sulfate is that in the CEM I plus added anhydrite. The sulfate in mix designation L is that in the CEM I only.

2.2. Methods

Compressive strength was measured in accordance with EN 196-1. Mortar prisms, 40x40x160 mm were made from 1 part of cement to 3 parts of sand at 0.5 w/b ratio using a 5-litre capacity digital mixer. The prisms were demolded after 24 hours and immediately stored in water at 20 °C until testing. Six test specimens, obtained from splitting the prims into halves were tested at selected ages up to 90 days.

To clarify the compressive strength evolution as a function of the sulfate content in the cements, hydration was followed, and microstructures were characterized, using paste samples. These were prepared according to the procedure for mortar preparation, as described in EN 196-1 but without

aggregates using a vortex mixer. The mortar samples were prepared on a 5-litre capacity digital mixer. Care was taken to ensure homogeneous mixing by additional hand mixing during the mixing breaks.

Isothermal calorimetry was conducted on 9.0 g of paste prepared with 0.5 w/b ratio. The heat of reaction was measured continuously for 28 days at 20 °C using an 8-channel TAM Air calorimeter. Reference channels were filled with ampoules containing 6 g of quartz mixed with 3 g of deionized water.

Chemical shrinkage was measured by dilatometry, with 15g of paste prepared with a 0.5 w/b ratio. The paste was mixed by hand for 2 minutes before being poured into a plastic beaker, 34 mm in diameter and 68 mm high. The beakers were tapped to level the paste and remove any entrapped air. The rest of the beaker was filled with deionized water, using a plastic syringe to minimize disturbance. The beaker was then sealed shut with a rubber stopper through which a 1mL pipette was passed; with water filling the pipette in the process. A few drops of paraffin oil dyed with 1-(methylamino) anthraquinone, was added on top of the water, acting as a tracer, to follow the total shrinkage. Chemical shrinkage was continuously measured with a 10 MP camera, automatically capturing an image every 5 minutes for 28 days, monitoring the height of the tracer in the pipette. The images were analyzed using Zeiss Axiovision analyzer.

For calorimetry and shrinkage, parallel measurements were performed on mixes in which slag was replaced with quartz of similar fineness. The objective here was to isolate the filler effect from the SCM reaction as done elsewhere [16].

Samples for XRD, TGA, SEM-EDS and MIP were cast into 15 ml plastic vials, sealed and rotated for the first 12 hours to prevent bleeding. The vials were then stored in a water bath at 20 ˚C until testing.

XRD scans were performed on freshly ground samples without hydration stopping. The data were acquired on a PANalytical MPD Pro using a CuKα anode operating at 40 kV and 40 mA equipped with an X'Celerator detector, over a range of 5-80 °2θ using a step size of 0.0334 °. Automatic incident divergence and fixed anti-scatter slits were used together with a 10 mm incident beam mask. The continuous scan mode was adopted for all data acquisitions. The data analysis was performed on TOPAS Academic software v4.2. The QXRD/ PONKCS method used to evaluate slag hydration is detailed elsewhere [18].

Specimens for TGA and MIP were hydration-stopped using the solvent exchange technique. The regime consisted of crushing the hydrated cement into 1 – 2 mm particles in isopropanol for 20 minutes, and filtering off the isopropanol under gravity in a glove-box which was kept free of CO_2 by purging with nitrogen gas. Maintaining the sample in the glovebox, the residue was rinsed with diethyl-ether before drying at 40 °C on a pre-heated glass plate for further 20 minutes. Following hydration stopping, samples were kept in mini-grip bags and stored in the glove-box until analysis.

TGA was performed on a Stanton Redcroft 780 Series Analyzer under nitrogen gas atmosphere, purged at 58 ml/min. About 16-18 mg of additionally ground powder sample was heated in a platinum crucible at a rate of 20 °C/minute up to 1000 °C. The bound water and portlandite contents were computed between 50-550 °C and ~400-500 °C from the TGA data using equations (1-2) respectively. The contents were then normalized to the ignited weight at 550 °C. The calcium carbonate content was also calculated from the TGA curve using equation 3 and the results normalized to the ignited weight at 1000 °C.

$$BW(\%) = \frac{(M_{50^oC} - M_{550^oC})}{M_{550^oC}} * 100\ \%\text{----------} (1)$$

$$CH(\%) = \frac{CH_{TG}\,{}^{74}/_{18}}{M_{550^oC}} * 100\ \% - - - - - - - (2)$$

$$Cc(\%) = \frac{Cc_{TG}\,{}^{100}/_{44}}{M_{1000^0C}} * 100\,\% ------- (3)$$

Where, BW is the bound water, CH is the portlandite content, CH_{TG} is % weight loss from water associated with calcium hydroxide, Cc is calcium carbonate content and Cc_{TG} is the weight loss associated with carbon dioxide, $M_{550℃}$ is the ignited weight at 550℃ and $M_{1000℃}$ is the ignited weight at 1000℃. Note that CH_{TG} and Cc_{TG} were calculated by the tangent method.

Total pore volume evolution was assessed from the TGA data using equation (4). We calculated the remaining water, not consumed by ongoing hydration, and normalized it to the initial volume of paste. The chemical shrinkage is considered at each stage of hydration according to the equation:

$$P\ (\%) = \frac{V_{por}}{V_{water} + V_{cement}} * 100\% = \frac{V_{water} - \frac{BW * M_{cement}}{1.\bar{3}\frac{g}{cm^3} * 100\%}}{V_{water} + \frac{M_{cement}}{\rho_{cement}}} * 100\% ----(4)$$

where P is the pore volume, V_{water} is the volume of the mixing or free water, V_{cement} is volume of cement, M_{water} is the mass of the mixing water per 100 g of cement ($V_{water} = M_{water}$ assuming density of 1 g/cm^3), M_{cement} is the initial cement mass, ρ_{cement} is the density of the cement, BW is the bound water content measured by the TGA at a given time and $1.\bar{3}$ g/cm^3 is the average density for chemically bound water assumed [20].

Samples for SEM-EDS were 2 mm thick discs cut from the paste cylinders using low speed Isomet saw and hydration stopped by freeze drying. The samples were resin impregnated and polished down to 0.25 µm using a combination of diamond paste and silicon carbide cloths. These were then carbon-coated under vacuum before the analysis. SEM/EDS analysis was performed in backscattered electron mode on a Zeiss EVO MA15 SEM equipped with an 80 mm^2 EDS detector. The instrument was operated at 15KeV accelerating voltage. EDS point analysis was also performed on the C-S-H and hydrated slag rims for the composition at 90 days. The Ca/Si ratio was obtained by plotting Al/Ca vs Si/Ca from 50 points and taking the high Si/Ca end of the cluster of EDS points; the Al/Si was taken as the slope of a line drawn from the origin and remaining tangential to the lowest cluster of points [21]. The S/Si ratio was similarly measured as the Al/Si ratio but after plotting the S/Ca versus Si/Ca atomic ratios.

MIP measurements were performed on 1 – 2 mm thick hydration-stopped samples using a Quantachrome Instruments' PoreMaster-60. Approximately 1 g of the sample was intruded with mercury at the rate of 6-19 MPa/min up to 400 MPa at 22 ºC. The intrusion data was converted to cumulative pore volume using the cylindrical and plate model together with the Washburn equation, taking the contact angle and the surface tension of mercury to be 140 º and the 0.48 N/m respectively. The data was analyzed in terms of the derivative of the cumulative curve after smoothening by the adjacent averaging method. It is noteworthy that crushing may induce micro-cracks and thus lead to potentially misleading results [22, 23]. However, such effects would be common to all investigated samples and hence may be discounted for comparative studies such as this. Additionally, the present study focused on the nanoscale. Consequently, micrometer level defects may not interfere significantly. The pore structure was characterized by the pore size distributions. The samples were frequently measured in duplicates and were found to be consistent.

Thermodynamic modeling was used to calculate the evolution of hydrate assemblages, from which hydrate volumes could be determined. This was carried out using the geochemical modelling program GEMS [24, 25] with thermodynamic data from the PSI-GEMS database [26, 27] supplemented by cement specific data [28-30]. The model was applied as described elsewhere [13]. The dissolution kinetics of anhydrous phases was mathematically described with multi-parametric smooth functions fitting the experimentally determined dissolution kinetics of clinker phases and slag. Hence, the composition of the hydrate assemblage was predicted based on the degree of reaction of the cement clinker and the slag as a function of time, assuming thermodynamic equilibrium at each stage of hydration. The following assumptions were introduced into the model:

- All anhydrous phases were assumed to dissolve congruently
- Calcite and gypsum contents were calculated to dissolve freely, i.e. without prescribing their dissolution degrees. Their amounts at equilibrium resulted from the availability of reacted alumina.
- C-S-H composition was corrected with Al and Sincorporation to account for Al-S-uptake determined experimentally, without altering its thermodynamic properties.

It should be noted that the volume of the C-S-H phase does not include the gel porosity associated with this phase, but only the interlayer water [30].

3. Results

3.1. Compressive strength

Compressive strength development in the cements is shown in Figure 2. Strength evolved slowly over the course of hydration as expected in composite cements. Sample S-3 showed the highest compressive strength while the lowest strength was measured in S-2 with the trends consistent throughout.

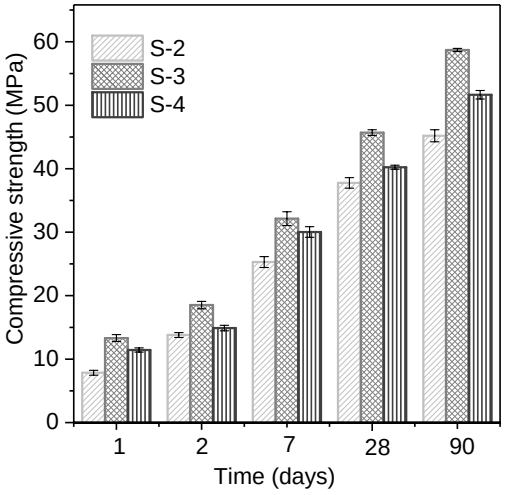

Figure 2 Compressive strength development over time for the three samples.

Consequently, under-sulfation (S-2) and over-sulfation (S-4) in ternary systems affected compressive strength negatively in a manner similar to other cement types reported elsewhere [6, 9, 10]. The remainder of this paper therefore explores the kinetic and microstructural effects which give further insight into the relationship between sulfate levels and compressive strength in ternary CEM I-slag-limestone cements.

3.2. Kinetics of hydration

3.2.1. Sulfates

The rate of heat evolution in the investigated cements is shown in Figure 3. The onset of the acceleration stage was independent of the sulfate content. The intensity of the silicate reaction peak (I) decreased slightly with increasing sulfate content, but this was because of the reduced overlap with the second effect (labelled as II). The peak labelled as II, which is associated with the depletion of sulfate [31, 32], showed the expected significant dependence on the sulfate content. It was retarded with the increasing sulfate content, with its maximum being after 12, 32 and 60 hours at 2, 3 and 4 % sulfate contents, respectively.

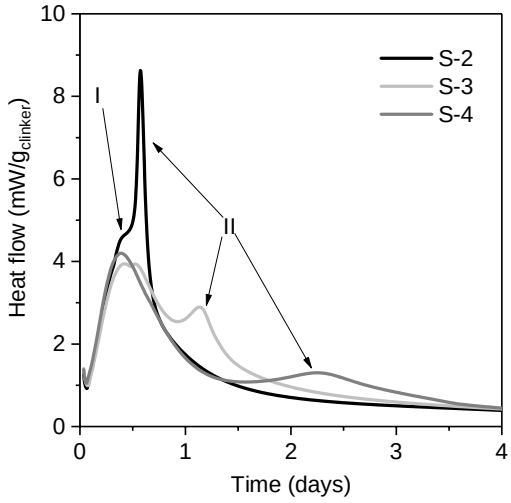

Figure 3 Isothermal calorimetry results of investigated cements

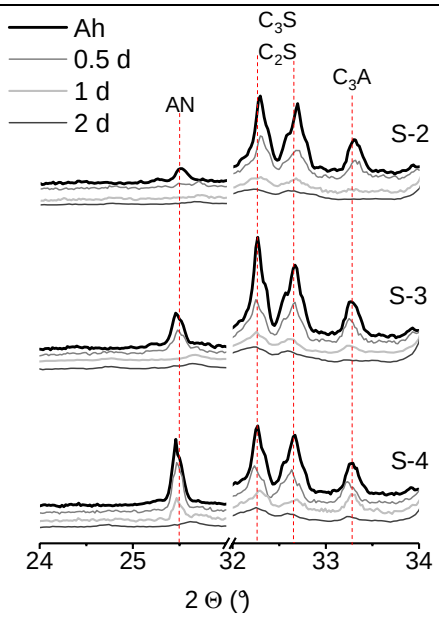

Figure 4 Effect of sulfate addition on the reaction of chosen cement components at early times; XRD data. AN – anhydrite, C_3S, C_2S and C_3A, Ah is the anhydrous cement

The sulfate depletion peak indicated by calorimetry did not however correspond to the complete dissolution of calcium sulfates, which was shown by XRD to occur earlier in the hydration process (Figure 3). Potential explanation includes the persistence of sulfates in the pore solution for longer periods after physical dissolution [33]. During the initial stages of hydration, the high concentration of sulfate in the pore solution is stabilized by the presence of calcium sulfates leading to sulfate adsorption on the C-S-H. Once anhydrite is depleted, the sulfate concentration in the pore solution drops with sulfates desorbing from the C-S-H [32, 34]. The continuing desorption of sulfate delays the sulfate depletion/aluminate reaction peak (II). XRD data reveal that in the mix containing 2 % sulfate, the complete reaction of anhydrite had occurred within the first 12 hours. In the case of the samples S-3 and S-4, the complete anhydrite dissolution had already occurred within 1 and 2 days respectively (Figure 4). Hemihydrate and arcanite were present in the CEM I, in addition to the additional anhydrite. There was no trace of these in any diffraction patterns after 12 hours.

3.2.2. Clinker

Figure 4 indicated notable modifications in the hydration kinetics of the cement clinker phases by the sulfate addition. These were quantitatively analyzed by the Rietveld refinement method and the results shown in Figure 4.

Alite hydration was fast and was not significantly affected by the sulfate content, consistent with the rate of heat evolution curves (Figure 3). The hydration of belite was slower than that of alite, but the results suggested that, at later times, belite hydration was accelerated at lower sulfate contents. However, the observed differences were smaller than the measurement error. The reaction kinetics of C_3A were inversely proportional to the sulfate content. The observed differences were still within the error of the Rietveld calculations (Figure 4), but they were confirmed by the analysis of the XRD traces (Figure 4). Some C_3A reacted alongside the silicates in the first 12 hours (see Figure 3). While hydration of C_3A was visible in the XRD traces, it was also possible to observe that, distinct C_3A peaks were still present after 1 day in the 3 and 4 % sulfate mixes and after 2 days in the 4 % sulfate mix.

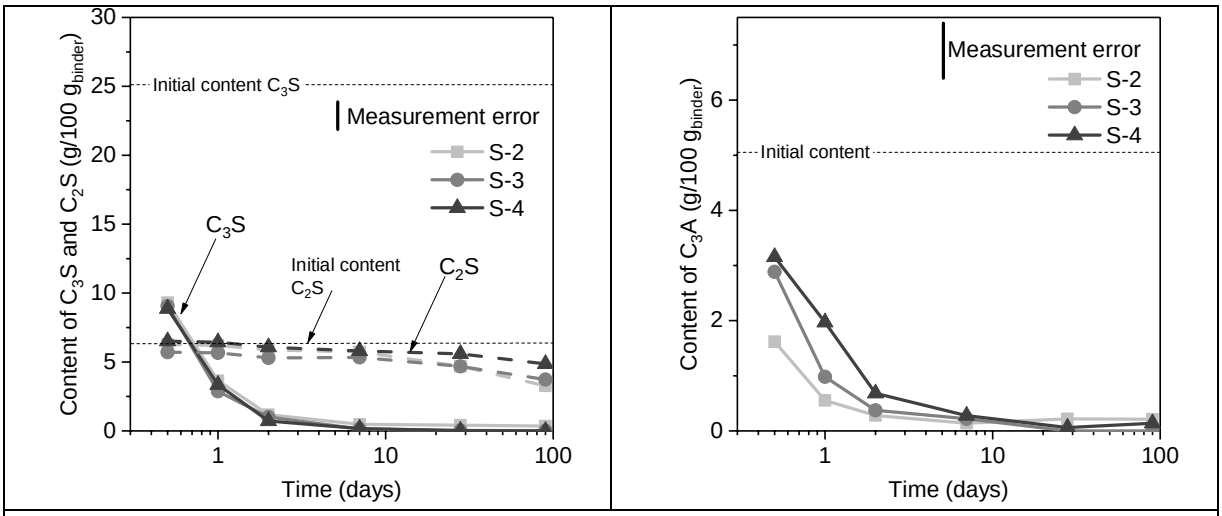

Figure 5 Effect of the sulfate dosage on the hydration of clinker phases. Note C_3S and C_2S (left) and C_3A (right). The error is estimated to be ±1 %.

The hydration degree of C_4AF is not discussed here since it was generally low (Table 2) and hence loaded with respectively high errors in the Rietveld calculations.

3.2.3. Slag

Chemical shrinkage is a semi-quantitative method suitable for determination of the degree of slag (or cement) hydration in composite cements of similar compositions [18, 35]. The filler effects associated with the presence of SCMs (F) and the active hydration of slag (S) in the three cements could be distinguished upon normalizing the data to the clinker contents (Figure 6). Chemical shrinkage indicated a greater degree of slag hydration in samples S-3 and S-4, compared to S-2, from about the third day of hydration. Earlier evaluation of slag hydration was not possible because of the occurrence of the effect associated with the sulfate depletion as for the calorimetry data shown in Figure 3. The QXRD/PONKCS method was employed to monitor slag hydration (Figure 6). Within the accuracy of the technique, a higher degree of slag hydration was measured at 3 % sulfate dosage while the lowest degree of hydration was measured in mix S-2, consistent with the chemical shrinkage results.

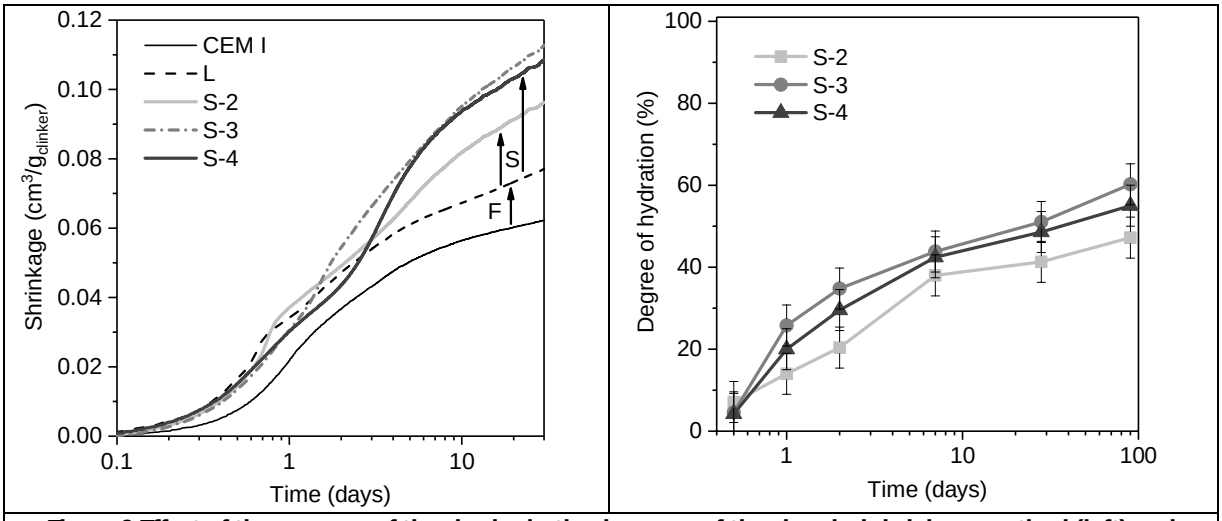

Figure 6 Effect of the progress of the slag hydration by mean of the chemical shrinkage method (left) and calculated by means of PONKS-Rietveld approach (right). S– is the active effect of slag, F is the filler effect. Note: L is the ternary CEM I-quartz-limestone mix and contained no additional sulfate other than was present in the CEM I. The error of Rietveld calculation is estimated to ± 5 % for slag.

3.2.4. Limestone

The calcite content was quantified from the TGA curve following the procedures described in [18] and the results shown in Figure 6. The reaction of calcite was limited to approximately 3 g per 100 g of binder over the first 90 days. The early reaction of calcite was retarded at higher sulfate contents, but the differences were generally smaller than the measurement error.

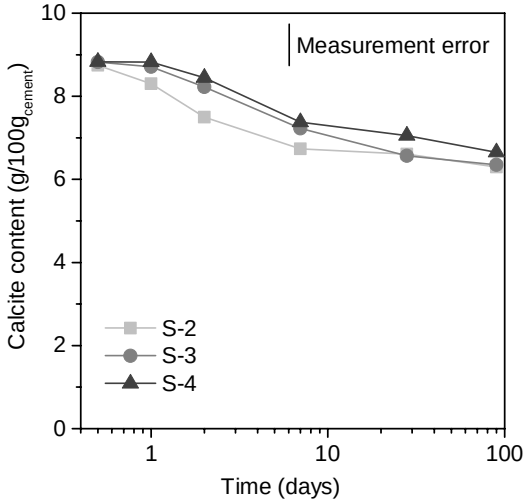

Figure 7 Evolution of calcite content in the investigated samples from TGA method. The error of the measurement is estimated ± 1 %

3.3. Evolution of hydrated phase assemblages

The thermodynamic modeling results (shown in Figure 8 for S-2 and S-4 as extreme cases) predicted C-(A)-S-H, ettringite, portlandite, hydrotalcite and carboaluminate as the main hydrates, irrespective of the sulfate dosage. As expected, more ettringite was predicted at higher sulfate contents, being stabilized over monosulfoaluminate due to the presence of calcite. Modeling closely predicted the bound water

content (Figure 9), plus the quantity of the crystalline phases; ettringite (Figure 10) and portlandite (Figure 11). Monocarboaluminate was predicted over hemicarboaluminate due to the thermodynamic stability [19]. A higher fraction of monocarboaluminate was predicted at lower sulfate levels.

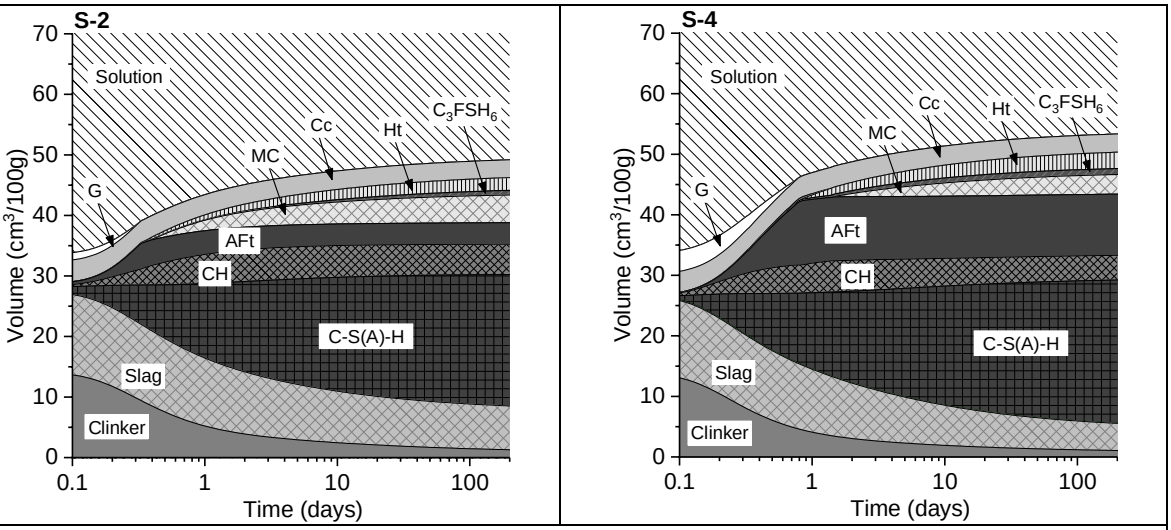

Figure 8 The volume of the different phases as function of time in hydrating cement pastes modelled by GEMS for samples with 2 % SO_3 (left) and 4 % SO_3 (right). C-S(A)-H - C-S-H phase with modelled incorporation of alumina, CH – portlandite, AFt – ettringite, MC – Monocarboaluminate, , Cc – calcite, Ht – hydrotalcite, C3FSH6 – iron containing hydrogarnets, G – gypsum.

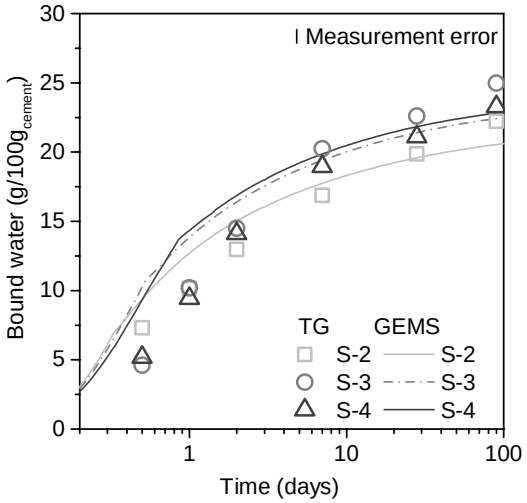

Figure 9 Bound water content over the hydration time; Points - TGA method results, error of measurement is estimated to be ± 1 %, Lines – results of the thermodynamic modelling

3.3.1. AFt/ AFm phases

The quantitative evaluation of the crystalline AFt/AFm assemblages based on Rietveld in addition to the thermodynamic calculations are shown in Figure 10. Considering the measurement accuracy (±1%), similar amounts of ettringite were formed after 12 hours, irrespective of the initial sulfate content (Figure 10 left). However, from 1 day onwards the ettringite contents were significantly different among the

mixes; being higher in the mixes containing more sulfate. After reaching a maximum, the ettringite contents did not change significantly with further hydration.

Figure 10 (right) indicate crystalline hemicarboaluminate was already present in the 2 % sulfate mix after 1 day, and then after 2 and 7 days in the 3 and 4 % sulfate mixes respectively. Monocarboaluminate were formed alongside hemicarboaluminate. The sulfate content further impacted on the hemi- to monocarboaluminate balance over the course of hydration. The content of hemicarboaluminate was similar in the investigated samples (accounting for the accuracy of the QXRD method), however trends indicated higher contents in the samples with lower SO_3 content. The conversion to monocarboaluminate was accelerated compared to the mixes containing higher sulfate contents. The trends are consistent with the dissolution kinetics of calcite (Figure 7) such that carboaluminate formation is proportional to the extent of calcite dissolution, which varied inversely with the sulfate content. The early age kinetic effects seem to dominate the AFt/AFm balance such that, rapid C_3A dissolution in the sample S-2 promoted calcite reaction once there was no more sulfate. This, in turn led to increased carboaluminate formation.

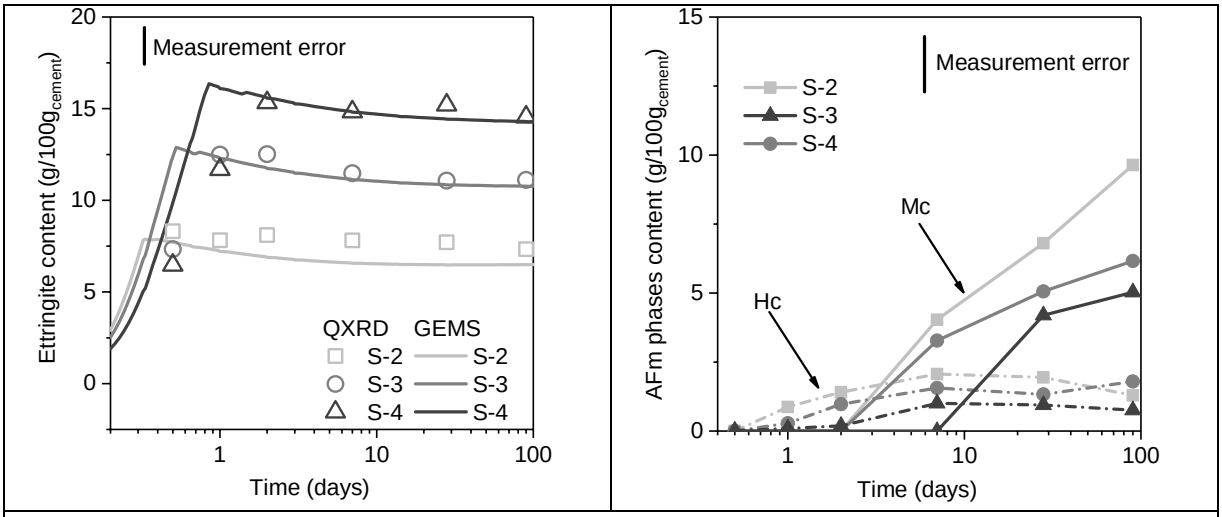

Figure 10 Evolution of ettringite (left) and AFm phases (right) over the hydration time. Points - QXRD method results, Error of measurement is estimated to be ± 1 % (highlighted in graphs), Lines – results of the thermodynamic modelling (only in the case of Ettringite; model does not predict correctly the type of phases presented ;most probably because of the kinetic hindrance [6])

It is noteworthy that as shown in Figure 8, the thermodynamic modelling predicts only monocarboaluminate. Consequently, direct comparison between the AFm contents from the modelling and Rietveld is not possible [6, 16]. Additionally, the AFm contents calculated by Rietveld are limited by their semi-crystalline nature [16].

3.3.2. C-S-H phase and Hydrotalcite composition

Molar Ca/Si, Al/Si and S/Si ratios of the C-S-H as measured by backscattered SEM-EDS are summarized in Table 5. Also shown is the Mg/Al ratio of the hydrotalcite phase, which was measured from the hydrated slag rim [36]. The C-S-H Ca/Si and S/Si ratios after 90 days increased with increasing sulfate content in the

sample. However, the Al/Si ratios were similar in all investigated samples. Meanwhile, the Mg/Al ratio varied with the sulfate dosage; being highest at the 3 % sulfate content.

Table 5 Molar ratios of the C-S-H and hydrotalcite composition after 90 days hydration as a function of the sulfate content (Note: ±2 % error associated with elemental analysis)

Mix	C-S-H			Hydrotalcite
	Ca/Si	Al/Si	S/Si	Mg/Al
S-2	1.66	0.12	0.05	2.1
S-3	1.71	0.11	0.07	2.6
S-4	1.72	0.11	0.09	2.4

3.3.3. Portlandite

The modelling data (Figure 11) indicate a marginally lower portlandite content with increasing sulfate content but the differences were not obvious from the TGA measurements. Notwithstanding, both sets of results pointed to a gradual decrease in the CH contents at longer hydration times. To understand these effects, the calcium incorporated into the crystalline ettringite and carboaluminate was calculated from the QXRD results, assuming stoichiometric hydrate composition. As illustrated in Figure 11, despite significant variations in the data over the course of hydration, the molar factions of calcium incorporated into the AFt/AFm were generally similar among the three cements at longer hydration times. Consequently, the decreasing portlandite contents may be caused by the consumption of Ca to form C-(A)-S-H or the increased slag reaction with the sulfate content.

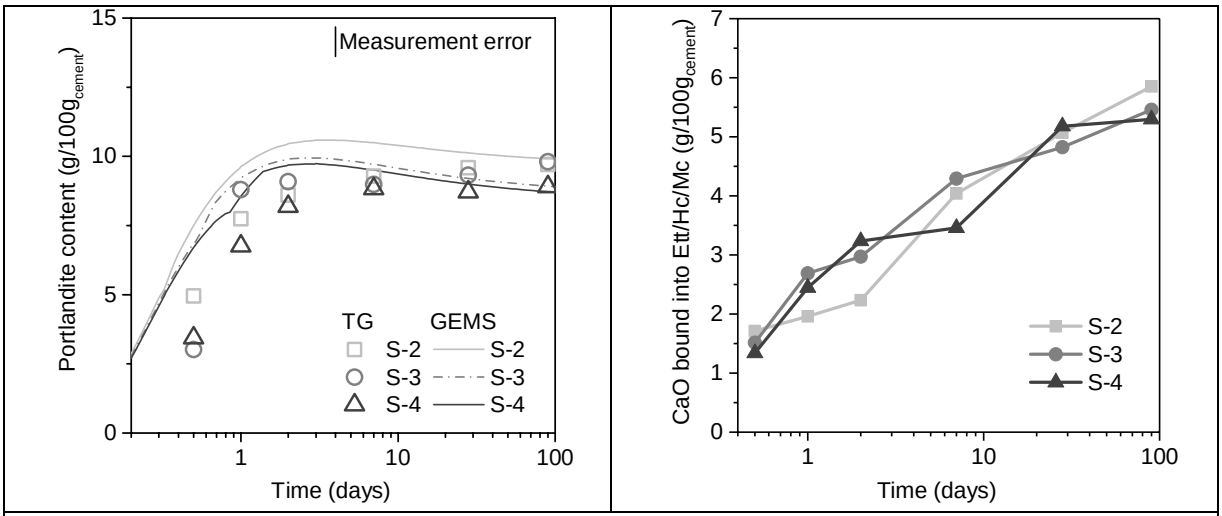

Figure 11 Portlandite content evolution over the hydration time (left); Points - TGA method results, Error of measurement is estimated to be ± 1 %, Lines – results of the thermodynamic modelling, and equivalent Ca bound into ettringite and carboaluminate (right)

3.4. Porosity

Mercury intrusion porosimetry was used to assess the samples' pore structures (Figure 12). With hydration, porosity refinement was observed. It is noticeable that the different sulfate content had no significant impact on the pore threshold diameter. However, it did change the distribution of the coarse

and fine porosity. At lower sulfate contents, there were fewer coarse pores and more fine pores (in the range 4 - ~20 nm), which can generally be associated with the C-S-H phase.

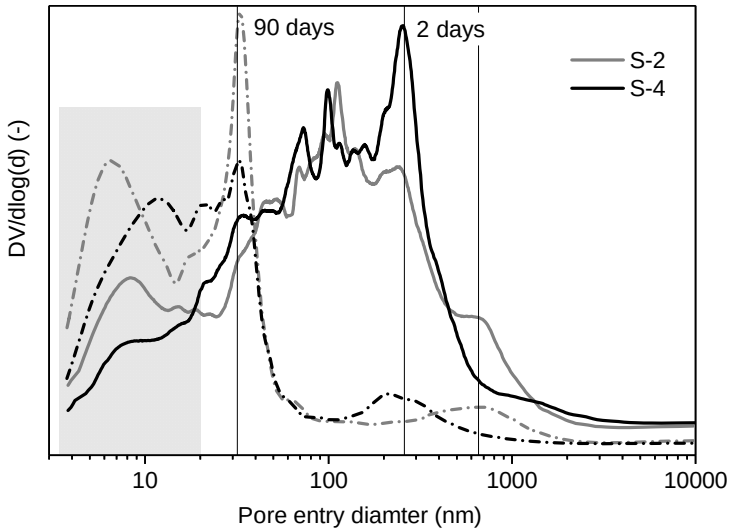

Figure 12 Pore size distribution in the chosen samples. Lines indicate the critical pore diameter at 2 and 90 days of hydration. Gray area highlight the fine porosity associated with the C-S-H phase. Note: Solid lines represent 2 days and dashed lines 90 days samples

Additionally, the total pore volume was assessed using the TGA method, as mentioned earlier (section 2.2). Figure 13 compares the results from the TGA method to those from thermodynamic modelling. MIP total porosity was not considered, since it is not a reliable technique for determining total porosity [37]. Generally, both methods showed a porosity decrease over time. Initially, the porosities were similar. But beyond 1 day they started to differ, depending on the sulfate level. GEMS showed a successively decreasing pore volume with increasing sulfate content. However, TGA suggested otherwise, with sample S-3 defined by the lowest pore volume, and sample S-2 by the highest.

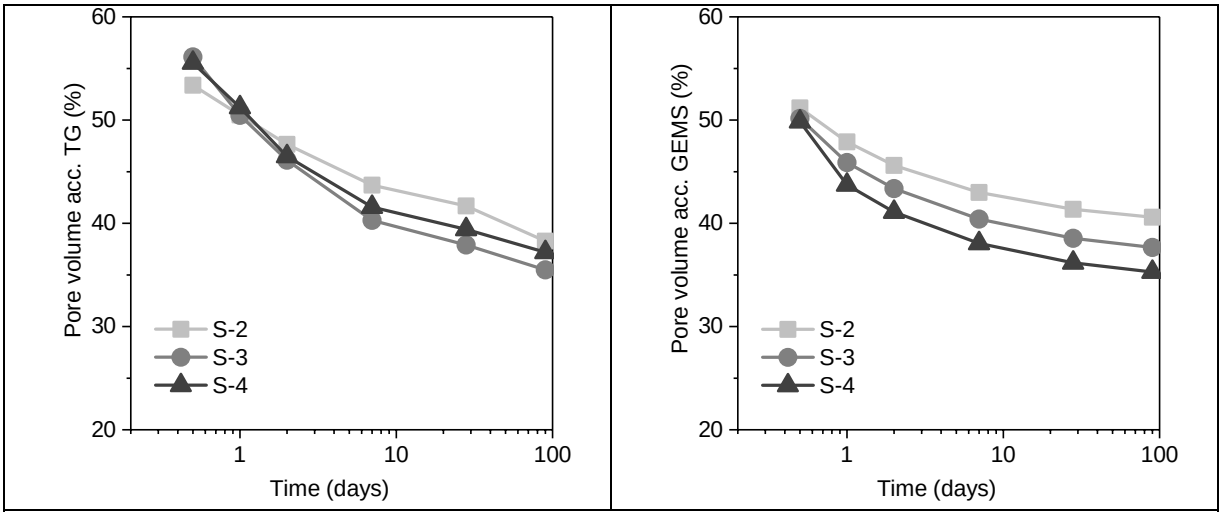

Figure 13 Total pore volume calculated from TGA (left) data and by GEMS (right)

4. Discussion

The sulfate content has multiple effects on the hydration kinetics and resulting phase assemblage. The calcium sulfate content significantly influences the early-age properties and continue to have a pronounced impact, even after the calcium sulfate is fully consumed.

4.1. Kinetics of hydration

An increasing calcium sulfate content has a pronounced impact on the early kinetics of C_3A hydration. This phase reacts more slowly while calcium sulfate is present, and accelerates once it is depleted [31, 32, 38]. The retardation mechanism is well recognized and related to the high sulfate concentration in the pore solution that is stabilized by the solubility of gypsum [2, 3]. The time to the complete depletion of the calcium sulfate is proportional to its content. Once it is depleted, acceleration of C_3A hydration is observed, for example by calorimetry (c.f Figure 3) or chemical shrinkage (c.f. Figure 6). It is noticeable that the feature within the calorimetry data associated with sulfate depletion correlates well with accelerated chemical shrinkage.

Besides C_3A, it has been suggested previously that sulfate accelerates the hydration of alite [6, 9, 10]. However, this effect has not been observed here (Figure 5). This is because we used finely ground CEM I 52.5R cement. Hence, alite reacts rapidly hydrating by over 60 % within 12 hours and 90 % within 1 day. Since sulfate is depleted within about 12 hours in S-2 and even later in the other samples (Figure 3), most of the alite reaction occurs in the presence of calcium sulfate and hence in a sulfate-bearing pore solution. Consequently, the potential impact of sulfate content on alite reaction cannot be observed.

However, changes could be seen in the rate of slag hydration. Increasing the sulfate content from 2 to 3 % accelerated the slag reaction (Figure 6), but a further increase in sulfate content to 4% had a minimal effect.

The acceleration of slag hydration may be explained by the change in pore solution concentration, or by the effect of sulfate on the microstructure. The lower sulfate content in the C-S-H of sample S-2, compared to S-3, indicates that the sulfate concentration in the pore solution is also lower, since the C-S-H phase composition is in close equilibrium with the pore solution [39]. Consequently, the higher reactivity may be an effect of the higher sulfate concentration. Note that Table 5 indicates little change in the Al/Si in the C-S-H, indicating a similar Al concentration in the pore solutions of all of the samples. This in turn excludes the effect described in [18], i.e. that lower Al concentration favours slag dissolution. Another possible explanation of this phenomenon is a change in the microstructure of the cementitious matrix. It is recognized that densification of the matrix leads to retardation of later-age reaction kinetics [40]. Here, the matrix is coarser at all times at higher sulfate levels, despite similar threshold pore diameters. Whittaker et al. [7] investigated the effect of sulfate, amongst other things, on similar systems, however using considerably lower limestone contents. They observed similar changes in C-S-H composition, plus similar porosity evolution, i.e. a decrease in the fine fraction and an increase in the coarse fraction. Similar to the results presented here, the total porosity calculated by GEMS was lower [41] as a result of the increase in sulfate content; from about 2 % to 4 %.

The XRD and TGA data indicate that the initial sulfate content modestly affected the reaction of calcite particularly at the early stages as it was evident through precipitation of hemicarboaluminate once sulfate was no longer present. The products of the reaction with calcite are hemi- and monocarboaluminate phases. Thermodynamic calculations indicate that monocarboaluminate is the stable AFm phase in all of

these systems, because of the high limestone, i.e. calcite, content (Figure 8). Meanwhile, XRD data show that it is hemicarboaluminate which forms initially, indicating kinetic hindrance, with hemicarboaluminate transforming slowly to monocarboaluminate (Figure 10). The quantities of hemi- and monocarboaluminate formed are related to the sulfate content of the cement. The sulfate content also affects the kinetics of carboaluminate formation; these being delayed by the presence of sulfate. However, the shape of the evolution in Figure 10 is the same for all of the samples investigated here. These findings further support the outcome of [18] that the kinetics of calcite reaction are limited by the availability of alumina and by the rate of formation of hemi- and monocarboaluminate.

4.2. Phase assemblages

The first and most obvious phenomenon observed with increasing sulfate levels is the increasing ettringite content and associated decrease of the AFm contents. This has been reported several times in the literature [7, 18]. However, it is interesting to note that the increase in ettringite content is limited by the adsorption of sulfate on the C-S-H, as shown in Table 5. Since these systems contain significant amounts of calcite, the ettringite is stabilized, even at later hydration times, in agreement with literature data [16, 19, 29]. As discussed above, higher sulfate levels retard the formation of hemicarboaluminate and monocarboaluminate. It is worth noting that, from the perspective of performance evolution, it is beneficial to increase the AFt to AFm ratio. This results in a lower total porosity because of the lower density of ettringite when compared to the AFm phases. The precise nature of the AFm phases, here being hemi- vs. monocarboaluminate, is of a secondary importance since their densities are similar.

The addition of more anhydrite leads to higher S/Si and Ca/Si atomic ratios in the C–S–H, as determined by EDS (Table 5) and consistent with the literature [6, 7]. These changes indicate that the different sulfate content has a pronounced impact on the cement paste properties well after the calcium sulfate is depleted:

- Different C-S-H composition indicates the different pore solution concentrations at later hydration times as discussed in the section "4.1 Kinetics of hydration"
- Varying Ca/Si has impact on the portlandite content in the investigated systems
- The increased content of S in C-S-H has a pronounced impact on the microstructure and water content of C-S-H phase and on the AFt/AFm ratio as discussed above.

The increased Ca/Si ratio of the C–S–H indicated that the decrease of portlandite content in the systems is related to the changes of the C-S-H phase composition. It is noticeable that independently of the sulfate content, the calcium bound in the AFt and AFm phases is similar, as shown in Figure 11. A similar increase in both the S/Si and Ca/Si ratios has been observed for different systems: in Portland cements [6, 7, 11], in C_3S [9] and in C–S–H - ettringite mixtures [42]. The simultaneous increase of Ca in the C–S–H indicates a coupled uptake of Ca and sulfate within the C–S–H [34]. Furthermore, the decrease of the portlandite content in the samples characterized by the higher sulfate level is as well related to the greater degree of slag hydration, as indicated by the thermodynamic modelling (Figure 11).

Sulfate content has a pronounced impact on the microstructure of the C-S-H phase. Several authors observed that an increase in the S/Si ratio in the C–S–H resulted in a decrease of the water content in the C–S–H and a clear decrease of the compressive strength of C_3S and C_2S samples [9-11, 43, 44]. Gunay et al. [10] indicated that the absorption of calcium sulfate on C–S–H results in a decrease of the forces between C–S–H particles which could be related to the decrease of the compressive strength of hydrated

alite pastes. Our results confirm these findings. Firstly, the MIP data indicate that the C-S-H phase in S-2 is characterized by a finer porosity compared to sample S-4. It is noticeable that these differences are visible from the second day of hydration. These differences are preserved till the end of experiments, i.e. at 90 days in our study. Analysis of the pore volumes (Figure 13) provides additional information about the C-S-H phase. Figure 14 plots the total porosities obtained by TGA against GEMS. The figure reveals differences in the relationships for the three samples. Since most of the other hydrates are crystalline and of well-defined composition (hydrotalcite content being low), the data suggest modification of the C-S-H microstructure in terms of the water content and hence the apparent density. Increasing the sulfate content increased the apparent density of the C-S-H. Adopting the appropriate density of the C-S-H (Table 6) for the calculation of the total porosity resulted in Figure 14 where a linear relationship was found between the porosity from GEMS and based on the TGA bound water. This confirms variations in the C-S-H composition and its water content as a function of the sulfate level.

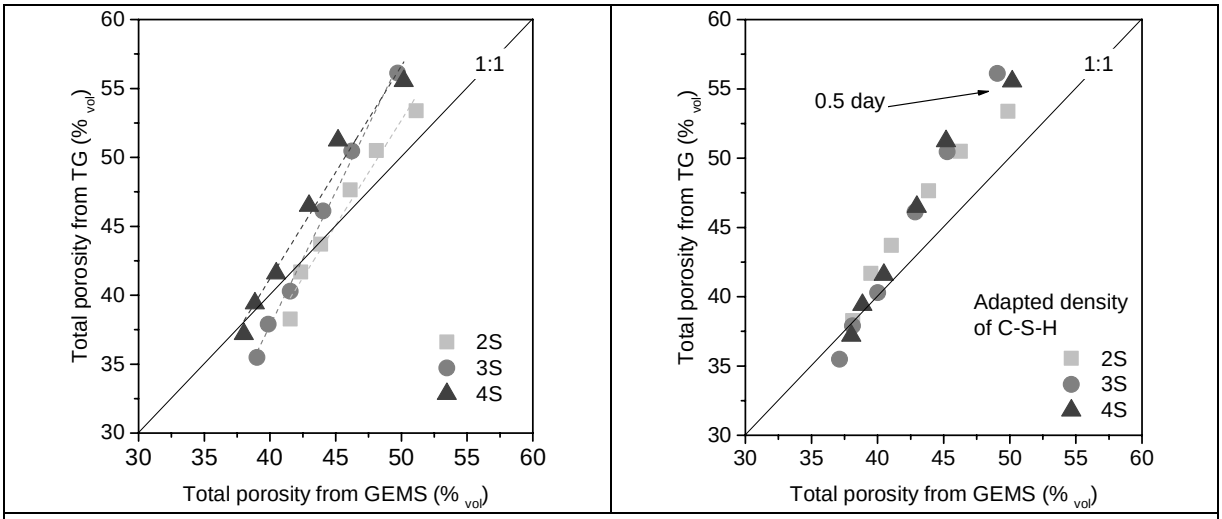

Figure 14 Comparison between porosity calculated from the TGA method and calculated by the GEMS; left the density of C-S-H as provided by GEMS (lines are guide for the eye), right; density corrected by the water addition to C-S-H phase.

Table 6 Modification of the C-S-H as a function of the sulfate dosage

Sample	Molar Si/H_2O	Apparent density (g/cm3)	Comment
S-2	2.9	2.2	Fitted
S-3	2.5	2.3	Fitted
S-4	2.0	2.4	As given by GEMS

4.3. Effect of phase assemblage on compressive strength

Increasing a cement's sulfate content results in an increase in the ettringite content (Figure 10) and a consequent porosity reduction, as predicted by thermodynamic modelling. This should result in an increased strength proportional to the sulfate content. However, mortar strength measurements showed that sample S-3 had the highest strength (c.f. Figure 13), while sample S-4, characterized by a higher

ettringite content, and had the lowest strength. This effect is readily explained by the effect of sulfate on the water content of C-S-H and its apparent density as shown in Figure 15.

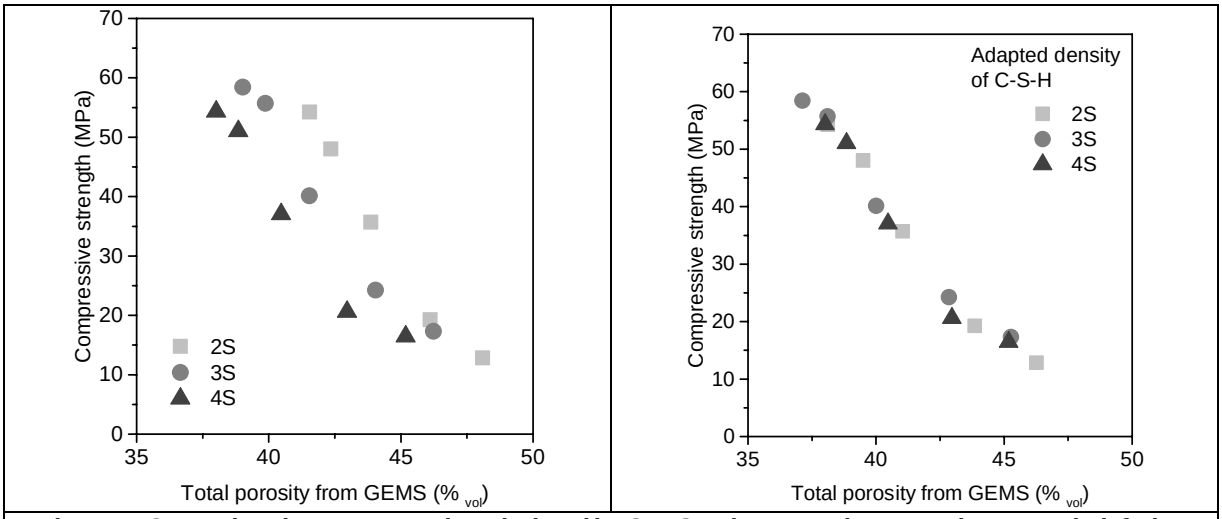

Figure 15 Comparison between porosity calculated by GEMS and measured compressive strength; left the density of C-S-H as provided by GEMS, right; density corrected by the water addition to C-S-H phase.

Consequently, the sulfate content has a two opposing effects on the compressive strength: increased volume of ettringite that increases the compressive strength and decreased density of the C-S-H phase that decreases the strength. The presence of these two contradictory phenomena clearly explains the need for the sulfate optimization that is the common practice in the cement industry.

5. Conclusions

The effect of sulfate dosage in ternary composite Portland clinker-slag-limestone cements has been investigated. The content of calcium sulfate has a pronounced impact on the reaction of the clinker phases and supplementary cementitious materials as well on the hydrate assemblages, hydrate properties and resulting cement performance. The results confirm the well-known effect of sulfate content on early-age properties, i.e. when calcium sulfate is still present. However, the results here also demonstrate that sulfate content also has a significant impact on the later-age properties of the hydrated cements.

The following conclusions are drawn based on the results of the present work:

- The sulfate content influenced the kinetics of clinker, slag and limestone hydration, though C_3S was not significantly affected.
- More ettringite was formed at the 4 % sulfate content while hemi and monocarboaluminate dominated at 2 %. The sulfate content ultimately determined the quantities of ettringite and carboaluminate formed.
- Finer pore structure was observed in the systems with lower sulfate levels.
- The sulfate dosage modified the microstructure and the properties of the C-S-H phase. The results points to changes in the water content of the C-S-H and hence of its apparent density.

Finally, this study reveals that increasing sulfates content modify paste microstructures in two opposing ways. Increased sulfate contents increase the volume of hydrates and thus the strength because of increased ettringite formation. Conversely, excess sulfate levels negatively impact on the performance of

C-S-H phase, which reduces the strength. This phenomenon appears as the common, occurring independently on the studied cement.

Acknowledgements

We thank the two anonymous reviewers for their invaluable suggestions. This work was funded by the University of Leeds. Additional financial and technical support was also provided by Heidelberg Cement, Leimen, Germany.

References

[1] Taylor HFW. Cement Chemistry. 2nd ed: Thomas Telford; 1997.
[2] Pourchet S, Regnaud L, Perez JP, Nonat A. Early C3A hydration in the presence of different kinds of calcium sulfate. Cement and Concrete Research. 2009;39(11):989-96.
[3] Minard H, Garrault S, Regnaud L, Nonat A. Mechanisms and parameters controlling the tricalcium aluminate reactivity in the presence of gypsum. Cement and Concrete Research. 2007;37(10):1418-26.
[4] Matschei T, Skapa R, Lothenbach B, Glasser FP. The distribution of sulfate in hydrated Portland cement paste. 12th Intern Congress on the Chemistry of Cements. Montreal, Canada2007.
[5] Lothenbach B, Matschei T, Möschner G, Glasser FP. Thermodynamic modelling of the effect of temperature on the hydration and porosity of Portland cement. Cement and Concrete Research. 2008;38(1):1-18.
[6] Zajac M, Rossberg A, Le Saout G, Lothenbach B. Influence of limestone and anhydrite on the hydration of Portland cements. Cement and Concrete Composites. 2014;46(0):99-108.
[7] Whittaker M, Zajac M, Ben Haha M, Bullergahn F, Black L. The role of the alumina content of slag, plus the presence of additional sulfate on the hydration and microstructure of Portland cement-slag blends. Cement and Concrete Research. 2014;66:91-101.
[8] Soroka I, Abayneh M. Effect of gypsum on properties and internal structure of PC paste. Cement and Concrete Research. 1986;16(4):495-504.
[9] Bentur A. Effect of Gypsum on the Hydration and Strength of C3S Pastes. American Ceramic Society. 1976;59(5-6):210-3.
[10] Gunay S, Garrault S, Nonat A, Termkhajornkit P. Influence of calcium sulphate on hydration and mechanical strength of tricalcium silicate. Intern Congress on the Chemistry of Cements. Madrid, Spain2011. p. 3-8.
[11] Copeland L. Kantro: Hydration of Portland cement. Proc 5th Intern Congress on the Chemistry of Cements. Tokyo, Japan1968. p. 387-421.
[12] Durdziński PT, Ben Haha M, Zajac M, Scrivener KL. Phase assemblage of composite cements. Cement and Concrete Research. 2017;99(Supplement C):172-82.
[13] De Weerdt K, Ben Haha M, Le Saout G, Kjellsen KO, Justnes H, Lothenbach B. Hydration mechanisms of ternary Portland cements containing limestone powder and fly ash. Cement and Concrete Research. 2011;41(3):279-91.
[14] Antoni M, Rossen J, Martirena F, Scrivener K. Cement substitution by a combination of metakaolin and limestone. Cement and Concrete Research. 2012;42(12):1579-89.
[15] Scrivener KL, Vanderley M. John, M. E. Eco-efficient cements: Potential, economically viable solutions for a low-CO2, cement based materials industry. 2016.
[16] Lothenbach B, Le Saout G, Gallucci E, Scrivener K. Influence of limestone on the hydration of Portland cements. Cement and Concrete Research. 2008;38(6):848-60.

[17] Schöler A, Lothenbach B, Winnefeld F, Zajac M. Hydration of quaternary Portland cement blends containing blast-furnace slag, siliceous fly ash and limestone powder. Cement and Concrete Composites. 2015;55:374-82.
[18] Adu-Amankwah S, Zajac M, Stabler C, Lothenbach B, Black L. Influence of limestone on the hydration of ternary slag cements. Cement and Concrete Research. 2017;100:96-109.
[19] Matschei T, Lothenbach B, Glasser FP. The role of calcium carbonate in cement hydration. Cement and Concrete Research. 2007;37(4):551-8.
[20] Powers TC, Brownyard TL. Studies of the physical properties of hardened Portland cement paste. Journal Proceedings1946. p. 101-32.
[21] Scrivener KL. Backscattered electron imaging of cementitious microstructures: understanding and quantification. Cement and Concrete Composites. 2004;26(8):935-45.
[22] Gallé C. Effect of drying on cement-based materials pore structure as identified by mercury intrusion porosimetry: A comparative study between oven-, vacuum-, and freeze-drying. Cement and Concrete Research. 2001;31(10):1467-77.
[23] Ma H. Mercury intrusion porosimetry in concrete technology: tips in measurement, pore structure parameter acquisition and application. Journal of porous materials. 2014;21(2):207-15.
[24] Kulik DA, Wagner T, Dmytrieva SV, Kosakowski G, Hingerl FF, Chudnenko KV, et al. GEM-Selektor geochemical modeling package: revised algorithm and GEMS3K numerical kernel for coupled simulation codes. Computational Geosciences. 2013;17(1):1-24.
[25] Wagner T, Kulik DA, Hingerl FF, Dmytrieva SV. GEM-Selektor geochemical modeling package: TSolMod Library and data interface for multicomponent phase models. The Canadian Mineralogist. 2012;50(5):1173-95.
[26] Hummel W, Berner U, Curti E, Pearson F, Thoenen T. Nagra/PSI chemical thermodynamic data base 01/01. Radiochimica Acta. 2002;90(9-11/2002):805-13.
[27] Hummel W, Berner U, Curti E, Pearson F, Thoenen T. Nagra Technical Report NTB 02-16. Wettingen Switz. 2002.
[28] Empa - 308 - Concrete/Construction Chemistry - Services.
[29] Matschei T, Lothenbach B, Glasser FP. Thermodynamic properties of Portland cement hydrates in the system CaO–Al 2 O 3–SiO 2–CaSO 4–CaCO 3–H 2 O. Cement and Concrete Research. 2007;37(10):1379-410.
[30] Kulik DA. Improving the structural consistency of C-S-H solid solution thermodynamic models. Cement and Concrete Research. 2011;41(5):477-95.
[31] Bullard JW, Jennings HM, Livingston RA, Nonat A, Scherer GW, Schweitzer JS, et al. Mechanisms of cement hydration. Cement and Concrete Research. 2011;41(12):1208-23.
[32] Scrivener KL, Juilland P, Monteiro PJM. Advances in understanding hydration of Portland cement. Cement and Concrete Research. 2015;78, Part A:38-56.
[33] Lothenbach B, Winnefeld F. Thermodynamic modelling of the hydration of Portland cement. Cement and Concrete Research. 2006;36(2):209-26.
[34] Barbarulo R, Peycelon H, Leclercq S. Chemical equilibria between C–S–H and ettringite, at 20 and 85 °C. Cement and Concrete Research. 2007;37(8):1176-81.
[35] Kocaba V, Gallucci E, Scrivener KL. Methods for determination of degree of reaction of slag in blended cement pastes. Cement and Concrete Research. 2012;42(3):511-25.
[36] Taylor R, Richardson I, Brydson R. Composition and microstructure of 20-year-old ordinary Portland cement–ground granulated blast-furnace slag blends containing 0 to 100% slag. Cement and Concrete Research. 2010;40(7):971-83.
[37] Zajac M, Skocek J, Adu-Amankwah S, Black L, Ben Haha M. Impact of microstructure on the performance of composite cements: why higher total porosity can result in higher strength. Submitted Cem Concr Compos.

[38] Quennoz A, Scrivener KL. Interactions between alite and C3A-gypsum hydrations in model cements. Cement and Concrete Research. 2013;44(Supplement C):46-54.
[39] Lothenbach B, Nonat A. Calcium silicate hydrates: Solid and liquid phase composition. Cement and Concrete Research. 2015;78, Part A:57-70.
[40] Berodier E, Scrivener K. Evolution of pore structure in blended systems. Cement and Concrete Research. 2015;73:25-35.
[41] Whittaker M, Zajac M, Ben Haha M, Black L. The impact of alumina availability on sulfate resistance of slag composite cements. Construction and Building Materials. 2016;119:356-69.
[42] Labbez C, Pochard I, Nonat A, Jönsson B. Colloidal Behavior of C-S-H Nanohydrates in Cement Paste. Symposium on concrete modelling (CONMOD 2010). Lausanne, Switzerland2010. p. 1-4.
[43] Kantro DL, Weise CH. Hydration of various beta-dicalcium silicate preparations. J Am Ceram Soc. 1979;62:621-6.
[44] Copeland L, Bodor E, Chang T, Weise CH. Reactions of tobermorite gel with aluminates, ferrites and sulfates. Portland Cement Association. 1967.